

GAS-KINETIC BGK METHOD FOR THREE-DIMENSIONAL COMPRESSIBLE FLOWS

by

Yeefeng Ruan* and Antony Jameson⁺
Stanford University, CA 94303

Gas-kinetic BGK scheme with symmetric limited positive (SLIP) method, which was developed by Xu and Jameson, is modified and extended to three-dimensional compressible flows for the first time. BGK scheme is an approximate Riemann solver that uses collisional Boltzmann equation as the governing equation for flow evolutions. To demonstrate the robustness and accuracy of the scheme, it is applied to some typical shock flows ranging from 1D to 3D, and the computational results are compared with the exact results or experimental results. The simplified steady state BGK method is used as the flux solver of Jameson's multi-grid, time-stepping FLO87 computer program for wing calculations. The results show that Gas-kinetic BGK scheme is an excellent shock-capturing method for subsonic and supersonic flows.

1. INTRODUCTION

The development of numerical schemes based on the kinetic theory for compressible flow simulations started in 1960s. Chu's method¹, based on the gas-kinetic BGK model, with discretized velocity space, is one of the earliest kinetic methods used for shock tube calculations. In the 1980's and 90's, many researchers have contributed to gas-kinetic schemes. Pullin² was the first to split the Maxwellian distribution into two parts and used the complete error function to obtain the numerical fluxes. The resulting scheme was named Equilibrium Flux Method (EFM). By applying upwind technique directly to the collisionless Boltzmann equation, Mandal³ and Deshpande derived the same scheme, which is named Kinetic Flux Vector Splitting (KFVS). Numerical schemes based on Boltzmann equation are called Boltzmann-type schemes.

A typical Godunov-type finite volume scheme has two stages: reconstruction stage for constructing initial cell-averaged values at cell interfaces and evolution stage for computing flow variables at later times by solving physical governing equations. Gas-kinetic schemes based on the Bhatnagar-Gross-Krook (BGK) model⁴ are new methods to model the gas evolution process by solving

the simplified Boltzmann equation. BGK-type schemes are different from other Boltzmann-type schemes, which solve the collisionless Boltzmann equation by neglecting the collision term of the Boltzmann equation. Because of the inclusion of the collision term of the Boltzmann equation, BGK-type schemes take into account the particle collisions in the whole gas evolution process within a time step, from which a time-dependent gas distribution function and the resulting numerical fluxes at the cell interface are obtained. Moreover, due to its specific governing equation, the BGK method gives Navier-Stokes solutions directly in smooth regions. In the discontinuous regions, the scheme provides a delicate dissipative mechanism to get a stable and crisp shock transition. Since the gas evolution process is a relaxation process from a non-equilibrium state to equilibrium one, the entropy condition is always satisfied by the BGK method. Due to the dissipative nature of BGK methods, rarefaction shock, carbuncle phenomena or odd-even decoupling have never been observed, although they occasionally appear in the other Godunov-type schemes. Finally, gas-kinetic BGK schemes are positivity-preserving, which makes certain that only positive densities and pressures are obtained from numerical computations.

The development of gas-kinetic BGK methods for compressible flow simulations and other applications has attracted much attention and become matured in the last decade. In 1993, Prendergast¹¹ and Xu first successfully used gas-kinetic BGK method to solve hydrodynamic equations. In 1995, Xu^{13,15,16,17} introduced Jameson's SLIP formulation^{5,6} to construct high-order BGK schemes. In 1998, Kim^{8,9,10} and Jameson developed the LED-BGK solver on

*Graduate Student, AIAA Student Member

+Professor, AIAA Member

Copyright ©2002 by the authors. Published by the American Institute of Aeronautics and Astronautics, Inc., with permission.

unstructured adaptive meshes. In 2000, Chae⁷ and Kim proposed a modified gas-kinetic BGK scheme by introducing the Prantl number correction into flux calculations. Lately Xu¹⁴ has used BGK schemes to solve shallow water equations, ideal MHD equations, and for chemical reactions.

In this paper, the authors will present numerical results of three-dimensional compressible flows with the gas-kinetic BGK method. This is the first time that the gas-kinetic BGK scheme has been used for three-dimensional flows, and the results show that the BGK scheme provides a very good tool for solving multidimensional flows, especially for flows with strong shock waves. The shock-capturing property of the BGK scheme makes it very attractive for subsonic and supersonic flow simulations.

2. NUMERICAL SCHEMES FOR CONSERVATION LAWS

To illustrate our approach we consider the one-dimensional hyperbolic system of conservation laws

$$u_t + f(u)_x = 0$$

where u is velocity and f is flux.

In constructing a finite volume scheme, we proceed in two steps: First, we introduce a small spatial scale, Δx , and we consider the corresponding average $\bar{u}(x, t)$ inside each cell:

$$x_i - \frac{\Delta x}{2} \leq x \leq x_i + \frac{\Delta x}{2} \text{ to be}$$

$$\bar{u}_t(x, t) + \frac{1}{\Delta x} \left[f(u(x + \frac{\Delta x}{2}, t)) - f(u(x - \frac{\Delta x}{2}, t)) \right] = 0$$

Next, we introduce a small time-step, Δt , and integrate over the slab $t \leq \tau \leq t + \Delta t$, Hence

$$\bar{u}(x, t + \Delta t) = \bar{u}(x, t) - \frac{1}{\Delta x} \left[\int_{\tau=t}^{t+\Delta t} f(u(x + \frac{\Delta x}{2}, \tau) d\tau - \int_{\tau=t}^{t+\Delta t} f(u(x - \frac{\Delta x}{2}, \tau) d\tau \right]$$

We end up with an equivalent reformulation of the conservation law. The first step is the variable reconstruction stage and the second step is the flux evolution stage.

Reconstruction Stage

In the reconstruction stage, to avoid generating spurious oscillations in the solutions, limiter is used to interpolate cell interface variables for higher order schemes. Jameson has developed a general symmetric limited positive (SLIP) formulation construction of limiters:

$$L(u, v) = \frac{1}{2}(u + v) \left(1 - \frac{|u - v|^q}{(|u| + |v|)^q} \right)$$

- For $q = 1$, the MinMod limiter is obtained
- For $q = 2$, Van Leer's limiter is obtained
- For $q = 3$ or larger, the higher-order SLIP method is obtained

Let $x_j = j\Delta x$ be a uniform mesh and Δx the mesh size. W_j, W_{j+1} are cell-averaged variables and $W_{j+\frac{1}{2}}, W_{j-\frac{1}{2}}$ are the interpolated values at cell interface. To second order accuracy, the interpolated values at the left and right state of the interface ($i = 1/2$) can be written as

$$W_{j+\frac{1}{2}}^L = W_j + \frac{1}{2} L(\Delta W_{j+\frac{1}{2}}, \Delta W_{j-\frac{1}{2}})$$

$$W_{j+\frac{1}{2}}^R = W_{j+1} - \frac{1}{2} L(\Delta W_{j+\frac{3}{2}}, \Delta W_{j+\frac{1}{2}})$$

where $L(u, v)$ is the nonlinear limiter.

Evolution Stage

The evolution stage is basically to solve a Riemann problem. This area has been well developed in the past decades: some well-known Riemann solvers for the cell-interface fluxes estimations are:

- The exact iterative solver

- Roe's approximate solver
- The Harten-Lax-VanLeer Einfeldt (HLL) solver

The exact Riemann solver is too costly, and Roe's approximate solver permits unphysical solutions such as expansion shock waves. In this study, a robust and accurate high-order evolution method based on gas-kinetic theory is used to construct the numerical fluxes across a cell interface. This gas-kinetic BGK scheme is not just a simple alternative to the Riemann solver or another upwinding method. It has abundant physical basis to describe the numerical fluid. It provides better solutions for compressible flows, especially for very strong shock flows and supersonic flows.

3. GAS-KINETIC BGK METHOD

Boltzmann Equation

Due to the unique form of the equilibrium distribution function g in classical statistical physics, at each point in space and time, there is a one to one correspondence between g and the macroscopic densities, e.g. mass, momentum and energy. So, from macroscopic flow variables at any point in space and time, we can construct a unique equilibrium state. However, in the real physical situation, the gas does not necessarily stay in the local thermodynamic equilibrium state, such as gas inside a shock or boundary layer, even though we can construct a local equilibrium state there from the corresponding macroscopic flow variables. Usually, we do not know the explicit form of the gas distribution function f in an extremely dissipative flow region, such as that inside a strong shock wave. What we know is the time evolution of f , the so-called the Boltzmann Equation, for one-dimensional flow,

$$f_t + uf_x = Q(f, f)$$

Here f is the real gas distribution function, and $Q(f, f)$ is the collision operator. From the physical constraints of the conservation of mass, momentum and energy during particle collisions, the following compatibility condition has to be satisfied,

$$\int \psi_\alpha Q(f, f) d\mathbf{u} d\xi = 0$$

where ψ_α is the vector of moments, its three-dimensional formula will be given later.

BGK Model of the Boltzmann Equation

One of the main functions of the particle collision is to drive the gas distribution function f back to the equilibrium state g corresponding to the local values of ρ , ρU and $\rho \mathcal{E}$. The collision theory assumes that during a time dt , a fraction of dt/τ of molecules in a given small volume undergoes collision, where τ is the average time interval between successive particle collisions for the same particle. The collision term in the BGK model alters the velocity-distribution function from f to g . This is equivalent to assuming that the rate of change (df/dt) of f due to collisions is $-(f - g)/\tau$. So the Boltzmann equation becomes

$$\frac{\partial f}{\partial t} + u \frac{\partial f}{\partial x} = -\frac{f - g}{\tau}$$

At the same time, due to the mass, momentum and energy conservation in particle collision, the collision term $(g - f)/\tau$ satisfies the compatibility condition,

$$\int \frac{g - f}{\tau} \psi_\alpha d\mathbf{u} d\xi = 0$$

The BGK model coincides in form with the equations in the theory of relaxation processes and is therefore sometimes called the relaxation model.

If τ is a local constant, the solution may be written as

$$f(x, t, u, \xi) = \frac{1}{\tau} \int_0^t g(x - u(t - t_0), t', u, \xi) e^{-(t-t')/\tau} dt' + e^{-(t-t_0)/\tau} f_0(x - u(t - t_0), t_0, u, \xi)$$

where f_0 is the real gas distribution function f at t_0 , and g is the equilibrium state in (x, t) .

4. BGK SCHEME FOR 3D FLOWS

In the finite volume method, the discretization is accomplished by dividing the flow into a large number of small sub-domains and by applying the conservation laws in the integral form

$$\frac{d}{dt} \int_{\Omega} U dV + \int_{\partial\Omega} F \cdot dS = 0 \quad (4.1)$$

to each sub-domain Ω with boundary $\partial\Omega$. In this equation U is the macroscopic state vector, defines as

$$U = \begin{pmatrix} \rho \\ P_x \\ P_y \\ P_z \\ \varepsilon \end{pmatrix} \quad (4.2)$$

where ρ , \bar{P} and ε are the mass, momentum, and energy density, and \bar{F} is the flux vector with components F_x , F_y and F_z in the three coordinate directions. In a gas-kinetic finite volume scheme the flux vectors across cell boundaries are constructed by computing the gas distribution function f . In three dimensions, the governing equation for f is described by BGK model, which is

$$f_t + uf_x + vf_y + wf_z = \frac{g-f}{\tau} \quad (4.3)$$

where f is a function of space (x, y, z) , time t , particle velocity (u, v, w) , and internal variable ξ with K degrees of freedom (i.e., $K=2$ for $\gamma=1.4$ diatomic gases in 3D). The relations between mass ρ , momentum \bar{P} , and energy ε densities with the distribution function f are

$$\begin{pmatrix} \rho \\ P_x \\ P_y \\ P_z \\ \varepsilon \end{pmatrix} = \int \psi_\alpha f d\Xi \quad (4.4)$$

where ψ_α is the vector of moments

$$\psi_\alpha = \begin{pmatrix} 1 \\ u \\ v \\ w \\ \frac{1}{2}(u^2 + v^2 + w^2 + \xi^2) \end{pmatrix} \quad (4.5)$$

and $d\Xi = dudvdw d\xi$ is the volume element in the phase space. The equilibrium state g in the BGK model has a Maxwellian distribution of

$$g = Ae^{-\lambda[(u-U)^2 + (v-V)^2 + (w-W)^2 + \xi^2]} \quad (4.6)$$

where U , V , and W are macroscopic gas velocities. From the physical constraint of the conservation of mass, momentum and energy during particle collisions, the following compatibility condition has to be satisfied,

$$\int \frac{(g-f)}{\tau} \psi_\alpha d\Xi = 0 \quad (4.7)$$

at any point in space and time. This will lead to three-dimensional Euler equations. Here $\frac{g-f}{\tau}$ is collision term of Boltzmann equation, and τ is collision time.

The general solution for f in equation (4.3) in three dimensions at the position of (x, y, z) and t is

$$f(x, y, z, t, u, v, w, \xi) = \frac{1}{\tau} \int_0^t g(x', y', z', t', u, v, w, \xi) e^{-(t-t')/\tau} dt' + e^{-t/\tau} f_0(x-ut, y-vt, z-wt) \quad (4.8)$$

where

$x' = x - u(t-t')$, $y' = y - v(t-t')$, $z' = z - w(t-t')$ are the trajectory of a particle motion, and f_0 is the initial non-equilibrium gas distribution f at the beginning of each step ($t=0$). Two unknowns g and f_0 must be determined in the above equation to obtain the solution f . In order to calculate the evolution of the macroscopic quantities in equation (4.4), equation (4.3) can be integrated over u , v , w , x , y , z , and t for a control volume defined by a mesh cell and a time step T . This requires the evaluation of fluxes across a boundary separating two cells in the x direction and, to simplify the notation, the point for evaluating fluxes at the cell boundary will be assumed at $(x=0, y=0, z=0)$.

Generally, f_0 and g can be expanded around the cell boundary as

$$f_0 = \begin{cases} g^l(1+a^l x + b^l y + c^l z), x < 0 \\ g^r(1+a^r x + b^r y + c^r z), x > 0 \end{cases} \quad (4.9)$$

and

$$g = g_0(1 + \bar{a}x + \bar{b}y + \bar{c}z + \bar{A}t) \quad (4.10)$$

where g^l , g^r , and g_0 are local Maxwellian distribution function. The dependence of a^l, b^l, \dots, \bar{A} on the particle velocity can be obtained from the Taylor expansion of a Maxwellian, which have the form

$$\begin{aligned} a^l &= a_1^l + a_2^l u + a_3^l v + a_4^l w + \\ &+ a_5^l (u^2 + v^2 + w^2 + \xi^2), \\ &\dots, \\ a^r &= a_1^r + a_2^r u + a_3^r v + a_4^r w + \\ &+ a_5^r (u^2 + v^2 + w^2 + \xi^2), \\ &\dots, \\ \bar{A} &= \bar{A}_1 + \bar{A}_2 u + \bar{A}_3 v + \bar{A}_4 w + \\ &+ \bar{A}_5 (u^2 + v^2 + w^2 + \xi^2), \end{aligned} \quad (4.11)$$

where all coefficients of $a_1, a_2, \dots, \bar{A}_5$ are local constants. The idea of interpolating f_0 separately at the regions of $x < 0$ and $x > 0$ follows from physical considerations: for a non-equilibrium gas flow, the physical quantities can change dramatically from place to place, such as across a shock front where the upstream and downstream gas distribution function f could be different Maxwellians.

In the following, the SLIP formulation, similar to that used for the linear advection equation, will be used for the interpolation of all initial mass, momentum, and energy densities in the x, y, and z directions, respectively. After implementing the limiters, the macroscopic variables can be obtained in the left and right sides separately,

$$\begin{pmatrix} \bar{\rho} \\ \bar{P}_x \\ \bar{P}_y \\ \bar{P}_z \\ \varepsilon \end{pmatrix} = \begin{pmatrix} \rho_0 + \rho_1 x + \rho_2 y + \rho_3 z \\ P_{x0} + P_{x1} x + P_{x2} y + P_{x3} z \\ P_{y0} + P_{y1} x + P_{y2} y + P_{y3} z \\ P_{z0} + P_{z1} x + P_{z2} y + P_{z3} z \\ \varepsilon_0 + \varepsilon_1 x + \varepsilon_2 y + \varepsilon_3 z \end{pmatrix} \quad (4.12)$$

where $\rho_1, \rho_2, \dots, \varepsilon_3$ are local constants. The expansions (4.9) and (4.12) are substituted into the moment equation (4.4) to yield

$$\begin{pmatrix} \bar{\rho} \\ \bar{P}_x \\ \bar{P}_y \\ \bar{P}_z \\ \varepsilon \end{pmatrix} = \int \psi_\alpha f_0 d\Xi \quad (4.13)$$

All the coefficients in f_0 can be obtained directly. Then, g_0 in equation (4.10) at $(x=0, y=0, z=0)$ can be evaluated automatically by taking the limit of equation (4.8) as $t \rightarrow 0$ and substituting it into equation (4.7) to obtain

$$\int g_0 \psi_\alpha d\Xi = \int_{t>0} \int g^l \psi_\alpha d\Xi + \int_{t<0} \int g^r \psi_\alpha d\Xi \quad (4.14)$$

The other terms of \bar{a} , \bar{b} , and \bar{c} in equation (4.10) at $t=0$ can be computed from the new mass, momentum, and energy interpolations which are continuous across the cell boundary in all three directions. Now, the only unknown term left in equation (24) is \bar{A} . This can be evaluated as follows by substituting equation (4.9) and equation (4.10) into equation (4.8), we get

$$\begin{aligned} f(0,0,0,t,u,v,w,\xi) &= (1 - e^{-t/\tau}) g_0 \\ &+ (\tau(-1 + e^{-t/\tau}) + t e^{-t/\tau}) (u\bar{a} + v\bar{b} + w\bar{c}) g \\ &+ \tau(t/\tau - 1 + e^{-t/\tau}) \bar{A} g_0 + e^{-t/\tau} f_0(-ut, -vt, -wt) \end{aligned} \quad (4.15)$$

with

$$f_0(-ut, -vt, -wt) = \begin{cases} g^l (1 - a^l ut - b^l vt - c^l wt), u > 0 \\ g^r (1 - a^r ut - b^r vt - c^r wt), u < 0 \end{cases}$$

Both f in equation (4.15) and g in equation (4.10) contain \bar{A} . After applying the condition (4.7) at $(x=0, y=0, z=0)$ and integrating it over the whole time step T , such as

$$\int_0^T \int (g - f) \psi_\alpha d\Xi dt = 0 \quad (4.16)$$

five moment equations of \bar{A} can be obtained, from which the five constants in \bar{A} of equation (4.11) can be

uniquely determined. Finally, the time-dependent numerical fluxes in the x-direction across the cell boundary can be computed as

$$F_x = \begin{pmatrix} F_\rho \\ F_{P_x} \\ F_{P_y} \\ F_{P_z} \\ F_\varepsilon \end{pmatrix} = \int u \begin{pmatrix} 1 \\ u \\ v \\ w \\ \frac{1}{2}(u^2 + v^2 + w^2 + \xi^2) \end{pmatrix} f(0,0,0,t,u,v,w,\xi) d\xi \quad (4.17)$$

The corresponding fluxes F_y and F_z in the y and z directions are similarly obtained by taking moments with v and w , respectively.

5. RESULTS AND ANALYSIS

In order to demonstrate the accuracy and robustness of gas-kinetic BGK schemes, we have used them to solve Euler equations and Navier-Stokes equations for 1D, 2D and 3D compressible flows with shock waves. Since the BGK method uses the collisional Boltzmann equation, which is good for both smooth areas and discontinues areas, it is an excellent shock-capturing scheme.

5.1 BGK Scheme for 1D and 2D Flows

From gas-kinetic theory, the collision time should depend on macroscopic flow variables, such as density and temperature. For calculations of the Euler equations, the collision time τ is composed of two parts,

$$\tau = C_1 \Delta t + \Delta t \text{Min}(1, C)$$

$$C = C_2 \frac{|\rho_l / \lambda_l - \rho_r / \lambda_r|}{|\rho_l / \lambda_l + \rho_r / \lambda_r|}$$

where ρ is density, λ is related to pressure, and Δt is the CFL time step. The first term on the right-hand side gives a limiting threshold for the collision time to avoid the blowing up the program, such as the evaluations of

$\Delta t / \tau$ and $e^{-\Delta t / \tau}$, it also provides background dissipation for the numerical fluid. The second term is related to the pressure jump in the reconstructed initial data, which introduces additional artificial dissipation if high pressure- gradients are present in the fluid. For shock tube test cases, numerical results are not sensitive to the choices of the values of C_1 and C_2 . In the following testing cases, $C_1 = 0.05$ and $C_2 = 5$ are chosen to do the computations.

Case 1: Sod Shock Tube

This test case is one dimensional shock tube problem with two different initial constant states in the left and right parts of the tube. It is a standard Riemann problem with a similarity solution. There are three waves: shock, contact discontinuity and rarefaction emerging from the location of the initial discontinuity. The results are shown in Figure 1 where the solid lines are the exact solutions. The test data are:

CFL = 0.4
Time = 4.0 sec.
Speed = 1.2

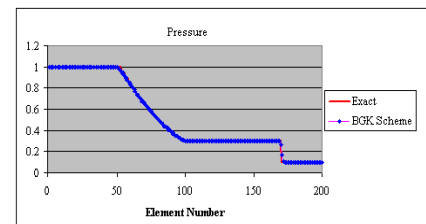
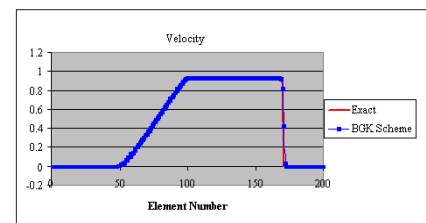
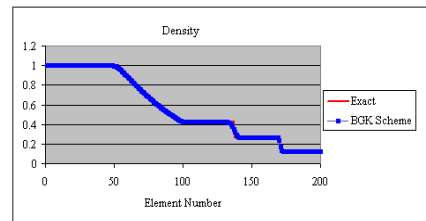


Figure 1. Results of Sod Shock Tube

Case 2: Lax-Harten Shock Tube

This is another Riemann problem that gives much stronger shocks and contact discontinuity waves than the Sod shock tube. The results are shown in Figure 2 where the solid lines are the exact solutions. The test data are:

CFL = 0.4
 Time = 2.0 sec.
 Speed = 2.65

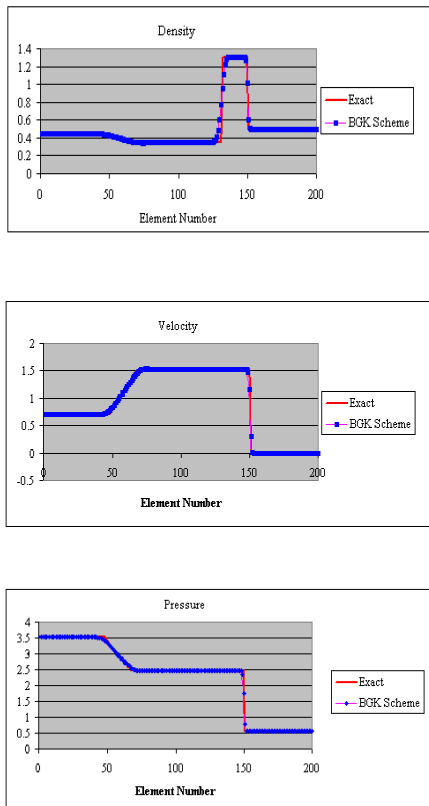


Figure 2. Results of Lax-Harten Shock Tube

Case 3: Woodward-Collela Shock

The initial condition consists of three constant states, each at rest between reflecting walls, separated by a distance of unity. Two strong blast waves develop and collide, producing new contact discontinuities. The

results are shown in Figure 3 where the solid lines are the exact solutions. The test data are:

CFL = 0.4
 Time = 0.038 sec.
 Number of elements = 400

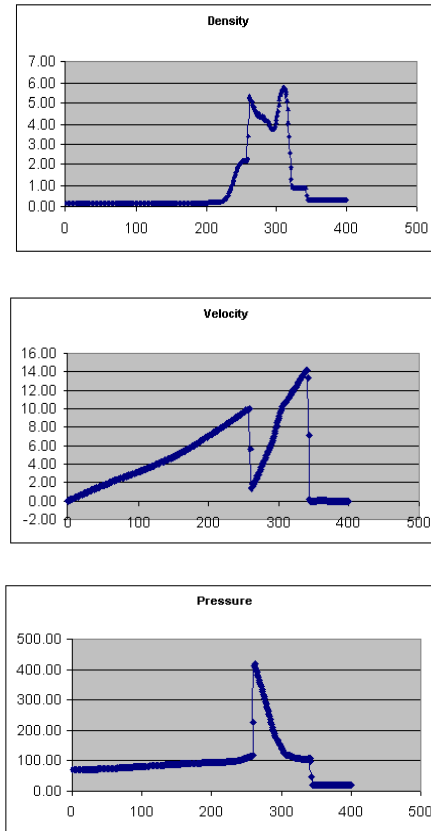


Figure 3. Results of Woodward-Collela Shock

Case 4: The interaction of an oblique shock wave with a laminar boundary layer

This is a classical shock/boundary layer interference problem that has attracted a lot of attentions of CFD community. It is to calculate the two dimensional viscous flow past a flat plate. An incident shock is coming in from top with an angle θ . The sketch of the flow is shown in Figure 4. The surface pressure and skin friction are shown in the top and bottom parts of Figure5 and 6. The results show that gas-kinetic BGK

schemes can catch the oblique shock and accurately predict the reverse flows inside the boundary layer.

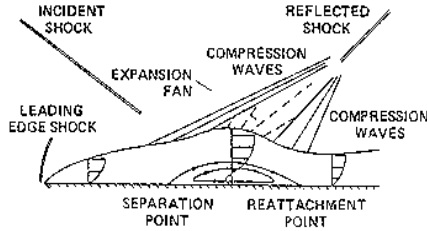


Figure 4. Shock/Boundary Layer Interaction Sketch

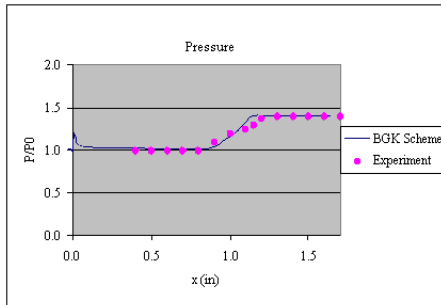


Figure 5. Surface Pressure of Shock/Boundary Layer Interaction

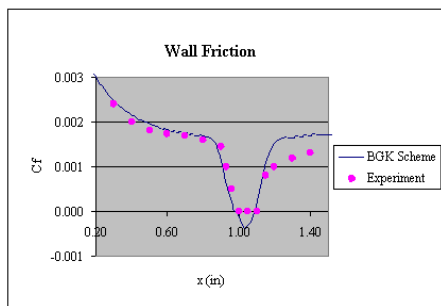


Figure 6. Skin Friction of Shock/Boundary Layer Interaction

Case 5: Double Mach reflection problem

It is generally known that schemes based on characteristic splitting with Roe averaging can produce the carbuncle phenomenon in steady or near-steady flows with a slowly moving shock. This phenomenon can be cured by increasing the artificial dissipation introduced with an entropy fix. The gas-kinetic BGK scheme produced a result without any symptom of the carbuncle phenomenon, which indicates that the BGK fluxes provide an appropriate amount of numerical dissipation. The density contour of this test case is shown in Figure 7.

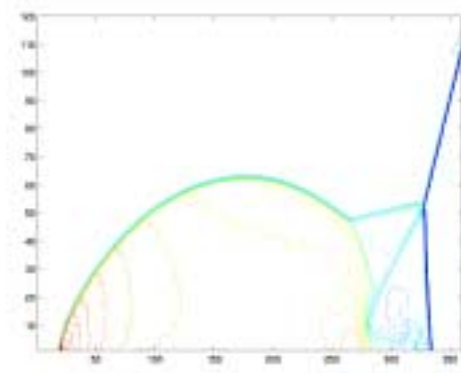


Figure 7. Density of Double Mach Reflection

5.2 BGK Scheme for 3D Wing Analysis

The full Boltzmann scheme gives time-dependent fluxes, which might handicap the convergence of the scheme to a steady state. Thus, for steady state calculations, the relaxation process must be simplified in order to yield constant numerical fluxes. The easiest way to achieve this is to ignore all high-order spatial and temporal terms in the expansion of f and g . So, instead of equation (4.9) and (4.10), we use

$$f_0 = \begin{cases} g^l, & x < 0 \\ g^r, & x > 0 \end{cases}$$

and

$$g = g_0$$

as the initial non-equilibrium gas distribution f_0 and the equilibrium state g . Substituting the above two equations into cell boundary can be obtained as

$$\begin{aligned} f(0,0,0,t) &= (1 - e^{-t/\tau})g_0 + e^{-t/\tau}f_0 \\ &= g_0 + e^{-t/\tau}(f_0 - g_0) \end{aligned}$$

The first term on the right hand side represents the Euler fluxes. The second term is a diffusive term, which should be large near discontinuities in order to keep f in a non-equilibrium state. This term is both necessary to prevent numerical oscillations and physically correct in that it accounts for the non-equilibrium behavior of the gas flow in the discontinuity region. This requirement makes $e^{-t/\tau}$ have the same functional effect as the parameter $\varepsilon^{(2)}$ in the JST scheme, which is controlled by a nonlinear limiting process.

Steady state transonic and supersonic flow calculations for NACA0012 and ONERA M6 wings using above simplified scheme are presented. In these calculations, the coefficient $e^{-t/\tau}$ in x direction (use subscript i) is as following

$$\varepsilon^{(2)} = e^{-t/\tau} = 1 - e^{-\alpha \text{Max}(P_{i+1}, P_i)}$$

where α is a constant, and

$$P_i = \frac{|\Delta p_{i+1/2} - \Delta p_{i-1/2}|}{|\Delta p_{i+1/2}| + |\Delta p_{i-1/2}|}$$

$$\Delta p_{i+1/2} = p_{i+1} - p_i$$

where p is pressure. In these wing calculations, the parameter is set to be $\alpha = 0.5$.

Extensive test cases have been run for wing calculations with a modification of Jameson's FLO87 program to incorporate the BGK scheme. The problems range from subsonic to supersonic flows for various angles of attack. Figure 8 shows the subsonic flow for wing with the NACA0012 section on a 192x32x48 mesh. The scheme successfully catches the strong shock at the upper surface at all sections of the wing. Figure 9 shows the result for supersonic flow over the NACA0012 wing. Shocks in front of the wing and behind the wing can be observed on the contour plot. Figures 10 and 11 show results of subsonic and supersonic flows for the ONERA M6 wing.

6. CONCLUDING REMARKS

Because of the complexity of its numerical formulation, the gas-kinetic BGK method has been limited to use only for 1D and 2D flows until now. Our results show that the steady state BGK scheme, with the help of convergence acceleration methods such as local time stepping and multi-grid technique, can calculate three-dimensional subsonic and supersonic flows accurately and efficiently. In order to compute three-dimensional hypersonic flows, the original gas-kinetic BGK scheme may be a better choice. This is the subject of ongoing research.

REFERENCES

- ¹C. K. Chu, Phys. Fluids, Vol.8, P12, 1965
- ²D. I. Pullin, *Direct Simulation Methods for Compressible Inviscid Ideal Gas Flow*, J. Comput. Phys., Vol34, P231-244, 1980
- ³J. C. Mandal and S. M. Deshpande, *Kinetic Flux Vector Splitting for Euler Equations*, Computers and Fluids, Vol23, No.2, P447, 1994
- ⁴P. L. Bhatnagar, E. P. Gross and M. Krook, *A Model for Collision Processes in Gases I: Small Amplitude Processes in Charged and Neutral One-Component Systems*, Phys. Rev., Vol94, P511-525, 1954
- ⁵A. Jameson, *Analysis and Design of Numerical Schemes for Gas Dynamics 1: Artificial Diffusion, Upwind Biasing, Limiters and Their Effect on Accuracy and Multigrid Convergence*, RIACS Technical Report 94.15, International Journal of Computational Fluid Dynamics, Vol.4, P171-218, 1995
- ⁶A. Jameson, *Analysis and Design of Numerical Schemes for Gas Dynamics 2: Artificial Diffusion, Upwind Biasing, Limiters and Their Effect on Accuracy and Multigrid Convergence*, RIACS Technical Report 94.16, International Journal of Computational Fluid Dynamics, Vol.5, P1-38, 1995
- ⁷D.S. Chae, C.A. Kim and O.H. Rho, *Development of an Improved Gas-Kinetic BGK Scheme for Inviscid and Viscous Flows*, J. Comput. Phys., Vol.158, P1-27, 2000
- ⁸C.A. Kim, *Robust and Accurate Numerical Methods for High Speed Unsteady Flows*, Ph.D Thesis, Princeton University, 1997

- ⁹C.A. Kim and A. Jameson, *A Robust and Accurate LED-BGK Solver on Unstructured Adaptive Meshes*, Accepted by J. Comput. Phys., 1997
- ¹⁰C.A. Kim, K. Xu, L. Martinelli, and A. Jameson, *Analysis and Implementation of the Gas-Kinetic BGK Scheme for Computational Gas Dynamics*, Int. J. Num. Met. In Fluids, 25, P21-49, 1997
- ¹¹K.H. Prendergast and K. Xu, *Numerical Hydrodynamics from Gas-Kinetic Theory*, J. of Comput. Phys. 109, P53, 1993
- ¹²T. Tang and K. Xu, *Gas-Kinetic Schemes from the Compressible Euler Equations. I: Positivity-Preserving Analysis*, 1997
- ¹³K. Xu, *Gas-Kinetic Schemes for Unsteady Compressible Flow Simulations*, VKI Report 1998-03, 1998
- ¹⁴K. Xu, *BGK-Based Scheme for Multicomponent Flow Calculations*, J. Comput. Phys., 134, P122-133, 1997
- ¹⁵K. Xu and A. Jameson, *Gas-Kinetic Relaxation Schemes for the Compressible Euler Equations*, AIAA 95-1736, 12th AIAA CFD Conference, 1995
- ¹⁶K. Xu, C. Kim, L. Martinelli and A. Jameson, *BGK-Based Schemes for the Simulation of Compressible Flow*, Int. J. Comput. Fluid Dynamics, 7, P213-235, 1996
- ¹⁷K. Xu, L. Martinelli and A. Jameson, *Gas-Kinetic Finite Volume Methods, Flux-Vector Splitting and Artificial Diffusion*, J. Comput. Phys., 120, P48-65, 1995

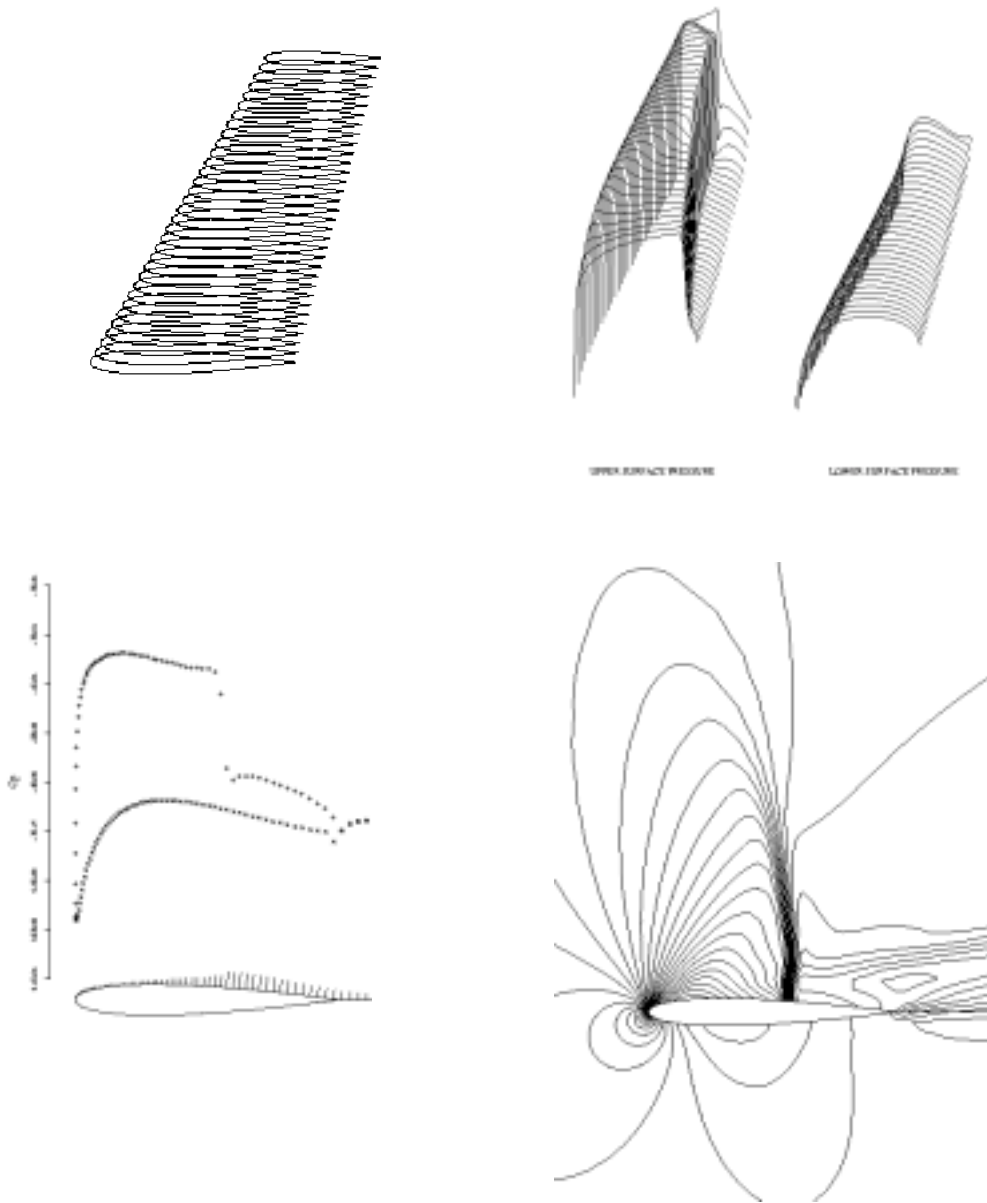


Figure 8. NACA0012 Wing Subsonic Flow

$$M = 0.84, \alpha = 9^\circ$$

Top: Pressures of Wing Upper & Lower Surfaces

Bottom Left: Root-Section Pressure Distribution

Bottom Right: Pressure Contour of Root-Section

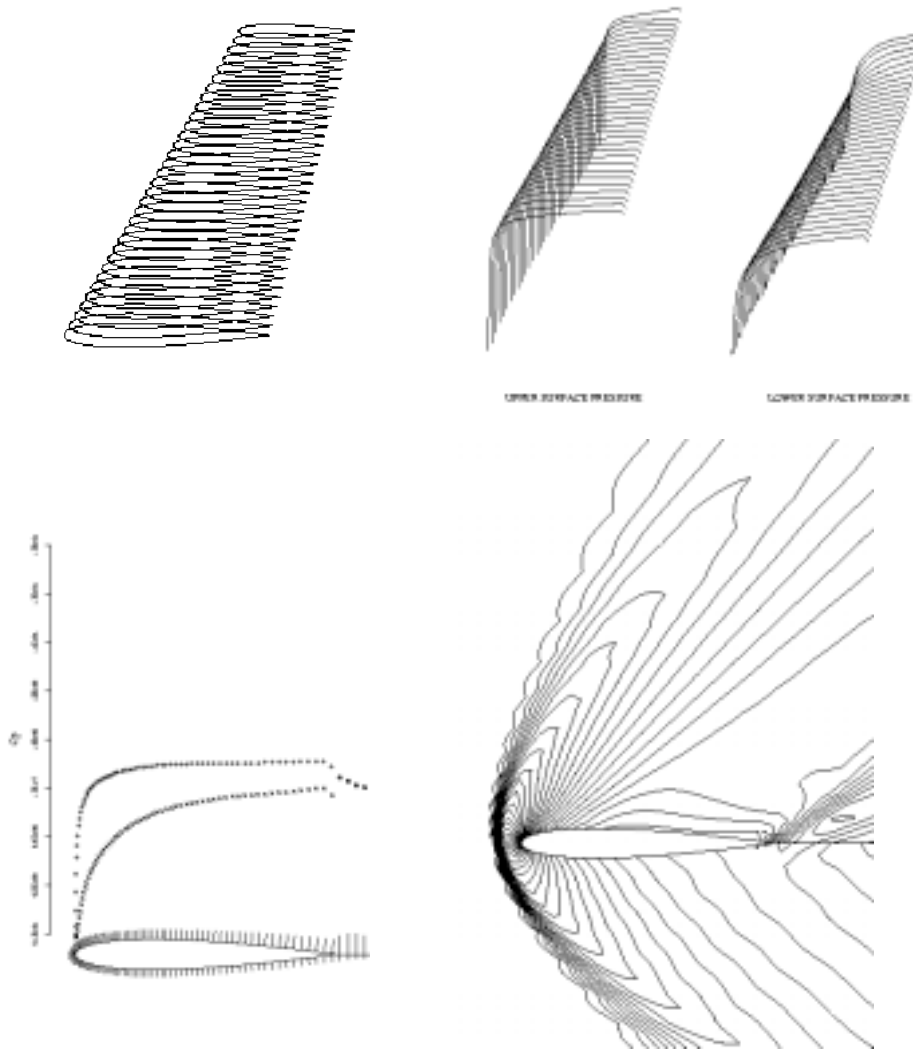


Figure 9. NACA0012 Wing Supersonic Flow
 $M = 2, \alpha = 11^\circ$
Top: Pressures of Wing Upper & Lower Surfaces
Bottom Left: Root-Section Pressure Distribution
Bottom Right: Pressure Contour of Root-Section

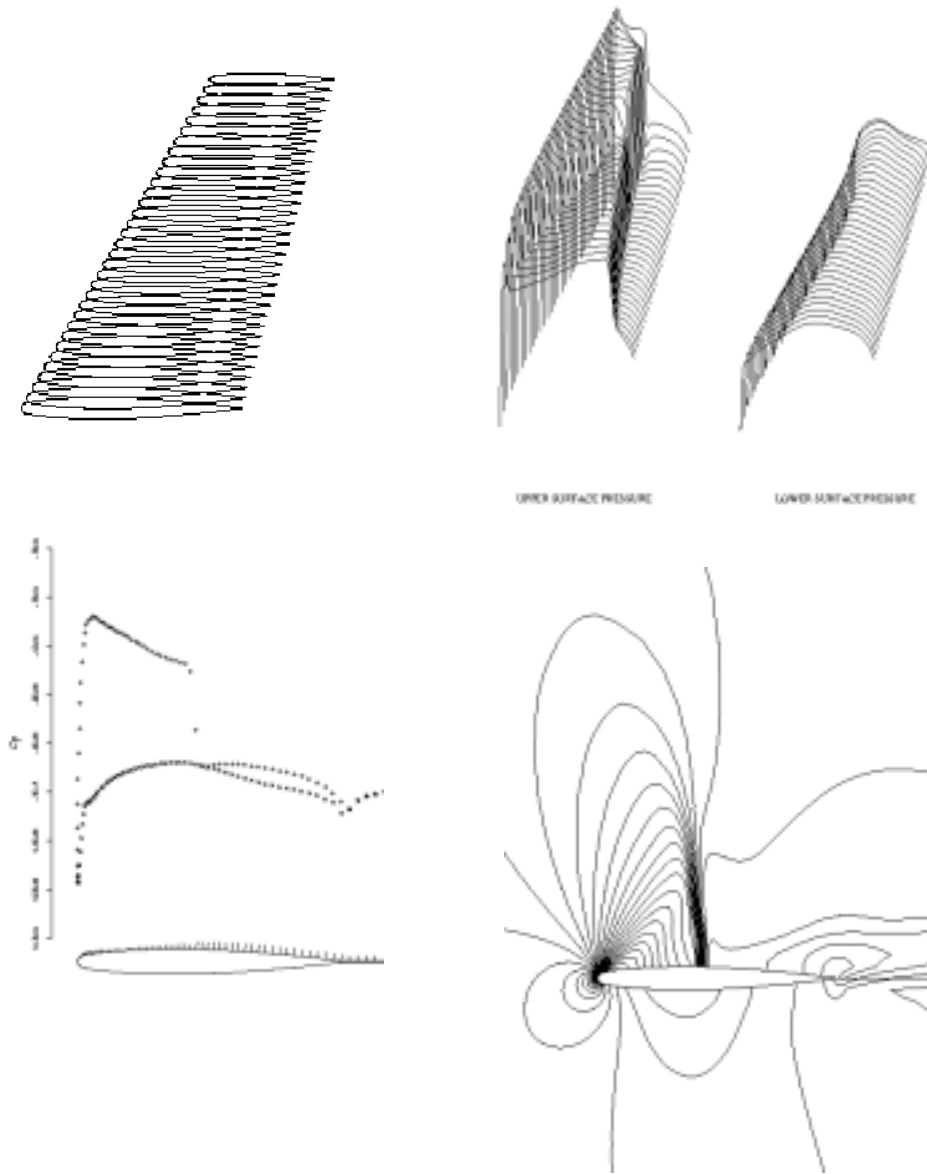


Figure 10. ONERA M6 Wing Subsonic Flow
 $M = 0.84, \alpha = 9^{\circ}$
Top: Pressures of Wing Upper & Lower Surfaces
Bottom Left: Root-Section Pressure Distribution
Bottom Right: Pressure Contour of Root-Section

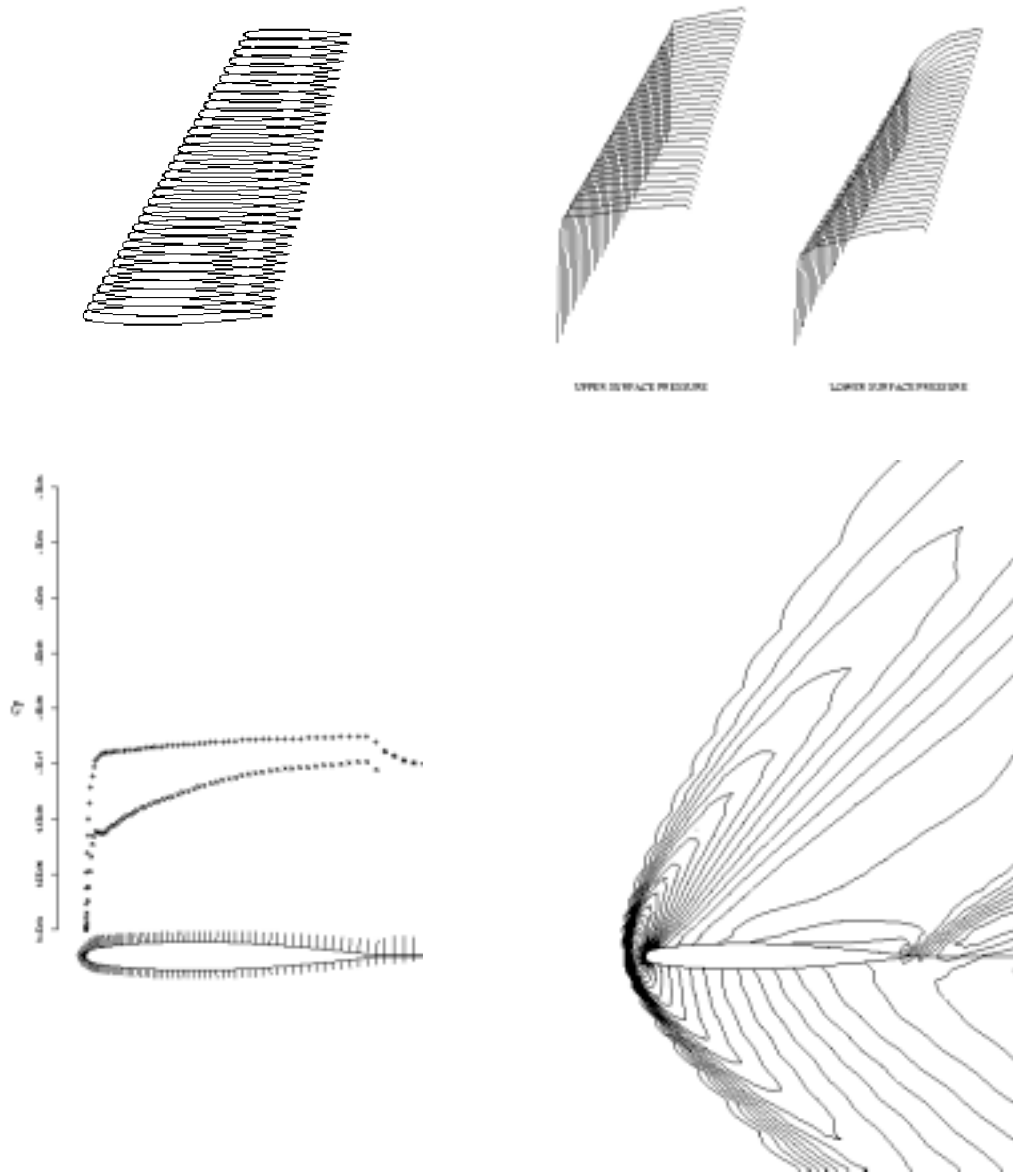


Figure 11. ONERA M6 Wing Supersonic Flow
 $M = 2, \alpha = 9^\circ$
Top: Pressures of Wing Upper & Lower Surfaces
Bottom Left: Root-Section Pressure Distribution
Bottom Right: Pressure Contour of Root-Section